energy&fuels

Open Access

pubs.acs.org/EF

Article

CO_2 Capture over Chitosan Biochars: Tailoring the Properties for Highly Efficient Adsorbents

Published as part of Energy & Fuels special issue "2025 Pioneers in Energy Research: Chunshan Song".

José A. O. Chagas, Bianca P. Pinto, Ana Lúcia de Lima, and Claudio J. A. Mota*

Cite This: https://doi.org/10.1021/acs.energyfuels.5c02026

Read Online

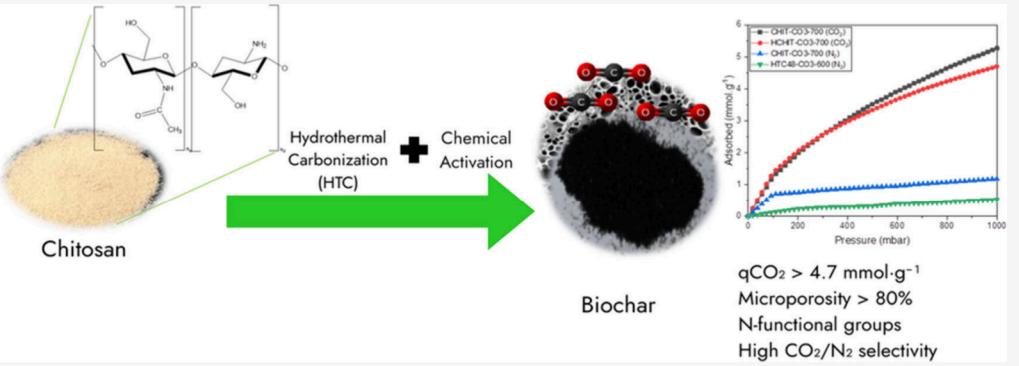

ABSTRACT: Chitosan biochars were prepared via two different pathways to obtain N-functionalized adsorbents. The direct calcination of chitosan in the presence of K_2CO_3 afforded CHIT-CO3-XXX materials (XXX refers to the temperature of calcination), whereas the initial hydrothermal carbonization (HTC) of chitosan, followed by calcination in the presence of K_2CO_3, afforded HTC48-CO3-XXX materials. The biochars obtained by direct carbonization of chitosan presented a lower BET area and nitrogen content than the carbons obtained from HTC chitosan, considering the same temperature of calcination. Among the biochars, CHIT-CO3-700 presented the highest CO_2 uptake (5.3 mmol·g^{-1}), whereas HTC48-CO3-600, prepared upon calcination of HTC chitosan, presented 4.7 mmol·g^{-1} of CO_2 uptake, at 25 °C and 1 bar. These materials were characterized by different techniques and tested for the adsorption of CO_2 at different temperatures. The adsorption profiles were better fitted by the Freundlich isotherm and the second-order kinetic model. The selectivity for CO_2/N_2 gas mixtures, taken from the Henry constant, was 1.7 and 10 for CHIT-CO3-700 and HTC48-CO3-600, respectively. *In situ* FTIR drift studies also indicated that the HTC48-CO3-600 biochar can retain some adsorbed CO_2 at 150 °C. These results may be explained by the higher total basicity of the HTC48-CO3-600 biochar, indicating that the initial hydrothermal carbonization of chitosan produces a biochar with improved properties for selective CO_2 capture.

1. INTRODUCTION

The processes of carbon capture and storage (CCS) and carbon capture and utilization (CCU) are gaining importance each day, due to global warming and international agreements to reduce carbon emissions in the forthcoming years.[1] The CO_2 capture from gaseous streams, especially from the burning of fossil fuels, or directly from the atmosphere (DAC),[2] are of prime importance to reduce the total CO_2 emissions and, together with other clean energy sources, would drive the planet toward the energetic sustainability until the end of the century.

The CO_2 capture using basic solutions is the most traditional technology.[3] Organic amines, such as monoethanol amine (MEA), are the most popular and widely used for this purpose.[4] However, they present some drawbacks, such as the high energy input to recover the CO_2 and regenerate the solvent, as well as corrosion of equipment and hazards associated with the manipulation and evaporation of the amines, which gradually reduce the absorption capacity and require continuous replacements, also impacting the costs. In addition, MEA is normally produced from fossil-derived feedstock,[5] making the process of absorption less sustainable in terms of the green chemistry principles.[6] On the other hand, CO_2 adsorption by solid sorbents is gaining interest,[7] because it is significantly less hazardous, may involve lower energy

Received: April 22, 2025
Revised: July 11, 2025
Accepted: July 14, 2025

input to recover the CO_2 molecule and may operate for prolonged periods without significant deactivation, thus reducing the operational costs. The main disadvantage is the total CO_2 uptake, which is generally lower compared to absorption by basic solvents. In addition, the materials that present the highest performance are normally expensive and difficult to use on a commercial scale.

Different types of adsorbents may be used for CO_2 adsorption, comprising high-surface area materials, such as metal organic frameworks (MOF),[8,9] zeolites,[10,11] aluminas,[12] and polymers,[13] among others. Depending on the nature of the material, the process may involve physisorption or chemisorption. Normally, high-surface area materials, such as MOFs and zeolites, capture the CO_2 molecule by physisorption, whereas on functionalized materials,[14] which present basic properties, chemisorption prevails. It is worth mentioning that for DAC applications, the CO_2 capture must involve chemisorption,[15,16] as the concentration of this gas is within 420−430 ppm, requiring highly selective materials.

Another important class of materials that have been used in CO_2 capture is activated carbon (AC).[17] For instance, Coromina and collaborators prepared porous biochars derived from different types of biomasses. Chemical activation with KOH led to high CO_2 adsorption under certain conditions.[18] For instance, calcination at 700 °C with a KOH impregnation ratio of 2 produced a material with around 5.0 mmol.g^{-1} of CO_2 uptake under ambient conditions. In a recent study, activated carbons prepared from olive wastes showed CO_2 uptake of 1.85 mmol·g^{-1}.[19] Other data indicated that AC prepared from sugar cane bagasse,[20] palm kernel shell[21] and coconut[22] show similar CO_2 uptake at 25 °C and 1 bar. Graphene-based adsorbents have also been studied for CO_2 capture.[23]

Park and collaborators prepared materials from carbonized chitosan, using urea as a nitrogen source and KOH as activating agent to generate porosity in the materials.[24] The prepared adsorbents presented surface areas varying from 368 to 2150 $m^2.g^{-1}$ and micropore volume from 0.225 to 1.302 $cm^3·g^{-1}$, with a CO_2 uptake of 6.37 mmol·g^{-1} at 0 °C and 3.91 mmol·g^{-1} at 25 °C, both at 1 bar of pressure. The authors highlighted the importance of micropores because under conditions of low CO_2 partial pressure, only adsorbents with a substantial amount of micropores can retain a significant volume of CO_2.

Fan and collaborators prepared microporous carbonaceous adsorbents through chemical activation at high temperatures, using chitosan as the precursor and K_2CO_3 as an activating agent.[25] The textural and chemical properties of the adsorbents can be adjusted upon variation of the K_2CO_3/chitosan ratio and activation temperature. The materials prepared with a K_2CO_3/chitosan ratio of 2 exhibited above 90% microporosity. The adsorbent prepared by calcination at 635 °C and a K_2CO_3/chitosan ratio of 2 showed a CO_2 uptake of 3.86 mmol.g^{-1} at 25 °C and 1 bar. The adsorption capacity remains almost constant upon five consecutive adsorption−desorption cycles, indicating that the material has great stability and recyclability. Furthermore, the result of N_2 adsorption was 0.18 mmol·g^{-1} at 25 °C and 1 bar, suggesting a good selectivity of this adsorbent for capturing CO_2 from nitrogen-rich gaseous streams.

Another class of chitosan-based biochar adsorbents was prepared using acetic acid as an additive through the combination of hydrothermal treatment and chemical activation with different proportions of KOH or NaOH as an activating agent. This procedure resulted in the formation of highly microporous materials of good selectivity for CO_2 adsorption in relation to N_2. The materials presented surface areas as high as 4168 $m^2·g^{-1}$. The adsorbents manufactured with KOH and NaOH showed CO_2 adsorption capacities of 8.36 mmol·g^{-1} at 0 °C and 1 bar.[26] The capacity of the biochars to capture CO_2 has been usually associated with the microporosity of the materials.[27]

Li and collaborators studied the CO_2 capture with nitrogen-doped chitosan biochars, employing activation with KOH under N_2 flow.[28] They found that the gas flow rate during activation affects the specific surface area and the total pore volume of the resulting carbons. The authors reported the importance of high N/C ratios, determined by XPS, in the CO_2 capture at low pressures. The presence of N atoms on the surface of the adsorbent can increase the affinity of the carbon materials for the CO_2 molecule, providing basic sites for the adsorption. Furthermore, the sample showed four successive adsorption−desorption runs, indicating remarkable recyclability.

Yogo and Fujiki prepared nitrogen-doped activated carbons from chitosan and alkali metal carbonates (Na_2CO_3, K_2CO_3, Rb_2CO_3 or Cs_2CO_3).[29] The materials exhibited CO_2 uptakes as high as 4.9 mmol·g^{-1} at 25 °C and 1 bar. Again, the effect of the microporosity of the materials was highlighted and associated with a better performance of the adsorbents. However, the CO_2 uptake at low pressure (0.01 bar) was strongly dependent on the nitrogen content of the materials, suggesting that the chemisorption of the CO_2 molecules on the basic sites may prevail at lower partial pressures.

It is possible to note that in the synthesis of chitosan-derived adsorbents, carbonization and pyrolysis are the most established methods, whereas chemical activation is effective in further improving the structural and textural properties, resulting in enhanced CO_2 adsorption capacity.[30] In most of the carbon materials reported in the literature, there is no significant functionalization to provide basic sites for more selective CO_2 capture. Functionalization might be achieved upon the use of ammonia during carbonization, yielding about 7.2 wt % of nitrogen atoms on the final activated carbon.[31] This led to 5.5 mmol·g^{-1} of CO_2 uptake at 25 °C and 1 bar. Another approach is the use of biomass-containing nitrogen atoms. Microporous biochars may be produced upon the carbonization and activation of crab shells, a biomass that has chitin in its composition.[32] The carbons presented nitrogen content between 5.1 and 8.5 wt % and exhibited a CO_2 adsorption capacity up to 4.37 mmol·g^{-1}.

We have studied chitosan-derived adsorbents for the CO_2 capture. Chitosan is a heteropolysaccharide with glucosamine units derived from the deacetylation of chitin (Figure 1). The hydrothermal carbonization (HTC) of chitosan afforded hydrochars that were able to capture up to 0.45 mmol·g^{-1} of CO_2.[33] This value is about 4-fold higher than the CO_2 uptake of pure chitosan under the same experimental conditions. Impregnation of chitosan on MCM-41 and SBA-15 mesoporous silica was also investigated.[34] The results showed that impregnation on the SBA-15 structure led to higher CO_2 uptake and were explained in terms of the micropore channels of the silica support, which allowed better diffusion of the CO_2 molecule to the chitosan impregnated on the mesopores.

In this work we employed the direct carbonization of chitosan as well as the carbonization of the hydrothermally

https://doi.org/10.1021/acs.energyfuels.5c02026
Energy Fuels XXXX, XXX, XXX−XXX

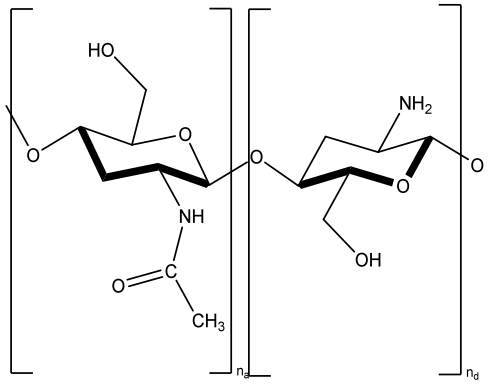

Figure 1. Structure of the chitosan polysaccharide.

carbonized biopolymer (HTC), together with chemical activation with K_2CO_3, to produce nitrogen-containing biochars. We conducted a comparative study of the properties and the CO_2 uptake of the carbon materials, also assessing the thermodynamic and kinetic analyses to better understand the main properties affecting the adsorption capacity of the chitosan biochar materials.

2. EXPERIMENTAL SECTION

The chitosan precursor was acquired from Polymar (Brazil) and had a deacetylation degree of 96%, estimated by CP/MAS ^{13}C NMR, and an average viscosimetric molar mass (M_v) of 1.7×10^5 g mol^{-1}. The K_2CO_3 was purchased from Vetec (Brazil). The CO_2 gas (99.99%) was obtained from Altec gases. All chemicals were analytical grade and used without further purification. The biochar materials were synthesized by two different methods: direct carbonization of chitosan (CHIT) or carbonization of the hydrothermally carbonized chitosan (HTC), which procedure of obtention was reported elsewhere.[33]

For the direct carbonization of chitosan, the general procedure starts upon mixing the chitosan with a 5.0 mol·L^{-1} solution of K_2CO_3, considering a chitosan/K_2CO_3 mass ratio of 1. The mixture was dried in an oven at 110 °C for 24 h, followed by calcination in two steps: from room temperature up to 300 °C at 8 °C min$^{-1,}$ and held at this temperature for 30 min under a N_2 atmosphere (50 mL.min^{-1}); then activation at the desired temperature (500−800 °C), at a rate of 10 °C.min^{-1}, for 60 min under flowing N_2. The samples were then thoroughly washed with hot water until neutral pH and dried at 110 °C for 4 h. The porous carbons produced were referred as CHIT-CO3-XXX, where XXX refers to the final calcination temperature (500, 600, 700, or 800 °C).

The CHIT-HTC48, which was prepared by hydrothermal carbonization of chitosan at 180 °C for 48 h,[33] was selected as starting material of the second procedure for the synthesis of chitosan biochars. The HTC material was mixed with a 5.0 mol·L^{-1} solution of K_2CO_3, considering a mass ratio of 1, and calcined through the same two-step procedure described before. The same washing and drying procedures were applied for the calcined HTC adsorbents, which were named as HTC48-CO3-XXX, where XXX refers to the final calcination temperature (500, 600, 700, or 800 °C).

The chemical composition of the biochars was determined by elemental analysis (CHN) on a PerkinElmer 2400 series II elemental analyzer. The chemical structure was characterized by Fourier Transform Infrared Spectroscopy (FTIR) in the range of 400−4000 cm^{-1} with a resolution of 2 cm^{-1} on a Shimadzu Iraffinity-1 equipment. The thermal stability was evaluated on a TGA-51 Shimadzu thermogravimetric equipment, from room temperature to 900 °C (10 °C.min^{-1}), under a N_2 atmosphere (50 mL.min^{-1}). The morphology of the carbons was analyzed by Scanning Electronic Miscroscopy (SEM), at a Phenon Pro X instrument, operated at an electron accelerating voltage of 10 kV. The textural properties of the samples were obtained from the nitrogen adsorption isotherms at −196 °C on a Micromeritics ASAP 2020 equipment. The biochars were treated at 180 °C under reduced pressure prior to the analysis.

The surface basicity of the parent materials and the biochars were evaluated by the Boehm method, a potentiometric acid−base titration. Initially, 40 mL of hydrochloric acid (0.1 mol·L^{-1}) were added to 0.2 g of the sample. The mixture was stirred for 24 h in a sealed flask and then filtered to remove the solid. Subsequently, 10 mL of the filtered HCl solution were added to 100 mL of distilled water and the system was titrated with a sodium hydroxide solution (NaOH, 0.1 mol·L^{-1}) under N_2 flow. The pH values were measured for every 0.5 mL of the titrant added to the system using a benchtop pHmeter. All measurements were performed in triplicate. The basicity was calculated according to eq 1, where the amount of residual acid was determined by the volume of the equivalence point, extracted from the second derivative of the potentiometric curve, and m is the mass of the material. The titration curves are shown in Figure S1 of the Supporting Information.

$$[OH^-] = \frac{n_{HCl,initial} - n_{HCl,residual}}{m} \quad (1)$$

The CO_2 adsorption isotherms were acquired on a XEMIS 100 gas sorption analyzer. The adsorption was carried out at 25 °C and up to 1000 mbar (100 mbar·min^{-1}) using pure CO_2. Prior to the adsorption analysis, each sample was pretreated for 4 h under vacuum at 180 °C. For selected samples, the CO_2 adsorption was studied in the temperature range of 0 to 60 °C to assess the thermodynamic parameters. The Langmuir and Freundlich linearized equations were used to describe the CO_2 adsorption isotherms. Thermodynamic parameters, such as enthalpy and entropy of adsorption and the isosteric heat, were determined using the Gibbs and Clausius−Clapeyron equations, respectively. The kinetic adsorption data were evaluated in real time during the experiments. The data was treated by the pseudo-first-order and pseudo-second-order models. The N_2 adsorption isotherms of selected biochars were also carried out at 25 °C and up to 1000 mbar, with the same pretreatment of the materials (180 °C, 4 h, under vacuum). The Henry constant (k) was obtained from the linearization of the adsorption data up to 200 mbar and was used to assess the selectivity for CO_2 and N_2 adsorption.

The XEMIS 100 gas sorption analyzer was also used in the flow mode to assess the adsorption properties of selected biochars for different N_2/CO_2 gas compositions. The materials were initially pretreated at 180 °C for 4 h under vacuum. Then, the system was cooled to room temperature, 350 mL.min^{-1} of gas flow containing N_2 and CO_2, in different molar proportions, were passed on the material, and the mass gain was monitored until constant weight for each gas composition.

In situ infrared drift studies of adsorbed CO_2 were conducted on a Shimadzu IRTracer100 spectrometer equipped with a diffuse reflectance Harrick cell, capable of operating under gas flow and high temperature. A sample of the biochar was initially pretreated at 150 °C under flowing N_2 (40 mL·min^{-1}). Then, the temperature was set to 25 °C and a flow of CO_2 diluted in N_2 (40 mL·min^{-1}) was passed through the sample, while infrared spectra were recorded. The temperature varied up to 150 °C to see the changes in the spectra.

3. RESULTS AND DISCUSSION

3.1. Characterization of the Biochars. The elemental compositions of the parent chitosan, the CHIT-HTC48 hydrochar, and the prepared biochars are shown in Table 1. The CHIT-HTC48 has a nitrogen content similar to chitosan, around 7.5 wt %, but the molar C/N atomic ratio is slightly higher, reflecting the effect of the hydrothermal treatment. As a general trend, the biochars presented higher carbon and lower nitrogen contents relative to the parent precursors. The C/N atomic ratio increases with the temperature of calcination, with the magnitude being higher for the materials obtained from the direct carbonization of chitosan (Figure 2). Thus, it seems that carrying out an initial HTC treatment favors the incorporation

https://doi.org/10.1021/acs.energyfuels.5c02026
Energy Fuels XXXX, XXX, XXX−XXX

Table 1. Chemical Composition of the Chitosan Biochars Obtained by CHN Analysis

sample	C (wt %)	H (wt %)	N (wt %)	C/N ratio[a]
chitosan	39.8	6.8	7.3	6.3
CHIT-CO3-500	55.0	3.3	7.1	9.0
CHIT-CO3-600	51.0	3.3	3.6	16.5
CHIT-CO3-700	50.2	3.7	1.7	34.5
CHIT-CO3-800	61.7	2.9	1.1	65.4
CHIT-HTC48	48.6	6.3	7.5	7.6
HTC48-CO3-500	63.0	2.4	8.4	8.8
HTC48-CO3-600	58.3	2.1	5.6	12.1
HTC48-CO3-700	55.4	2.7	2.3	28.1
HTC48-CO3-800	52.4	3.3	1.5	40.8

[a]Molar C/N ratio calculated from the CHN analysis.

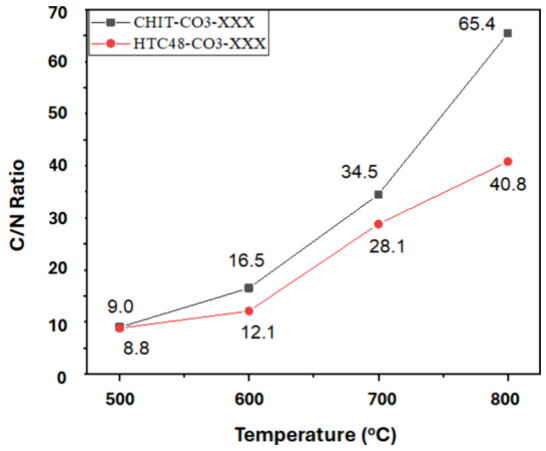

Figure 2. Atomic C/N ratio of the biochars as a function of the calcination temperature.

of more nitrogen atoms on the final biochar. The carbon content varied from 55.0 wt % to 61.7 wt %, and the nitrogen content from 7.1 wt % to 1.1 wt % in the biochars obtained directly from chitosan, whereas in the biochars prepared from the CHIT-HTC48 hydrochar the values were within 63.0 wt % to 52.4 and 8.4 wt % to 1.5 wt % for the carbon and nitrogen content, respectively. It must be stressed that all calcinations were carried out with an intermediate treatment at 300 °C for 30 min, before heating to the final desired temperature. This intermediate treatment seems to better preserve the nitrogen atoms in the final biochar materials.

The mineral content of the parent chitosan, CHIT-HTC48 hydrochar, and the produced biochars was around 1%, according to TGA measurements (Figures S2 and S3 of the supporting material).

Figure 3 shows the FTIR spectra of the chitosan biochars. All carbons showed bands in the range of 1750 to 1520 cm^{-1}, related to the C═C vibration of the aromatic systems overlapping with bands of C═O stretching and N−H deformation. Furthermore, in all spectra, there appear bands in the region between 1610 and 1480 cm^{-1}, associated with the -C═N vibrations, probably related to pyridine-like species, and between 1330 and 800 cm^{-1}, attributed to N-oxides. These species have been confirmed in carbons or products derived from the thermal decomposition of chitosan.[35]

It is clear from the FTIR spectra that upon increasing the final calcination temperature, the intensity of the C═O band near 1610 cm^{-1} decreases. This behavior was more significant

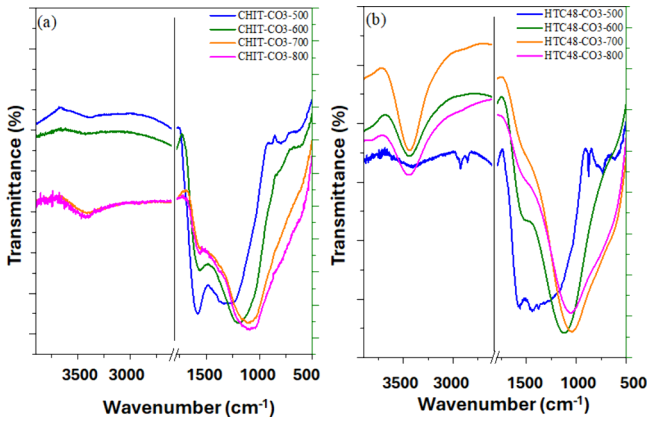

Figure 3. Infrared spectra of the biochars: (a) direct calcination of chitosan and (b) calcination of CHIT-HTC48 hydrochar.

in the HTC48-CO3 samples, in which a clear increase of the band centered at 3450 cm^{-1} was observed as the temperature of calcination goes up. This band may be associated with either N−H or O−H stretching, and it was generally more intense in the biochars produced from the CHIT-HTC48 hydrochar as starting material. Therefore, formation of N-pyridone and pyrrol-like species at higher calcination temperatures may be suggested for the HTC48-CO_3 adsorbents, but we cannot completely rule out that the bands may be due to amino groups, as the parent CHIT-HTC48 material also presents intense bands in this region.[33]

The N_2 adsorption isotherms are shown in Figure S4 of the Supporting Information. As previously seen, chitosan and CHIT-HTC48 present type II isotherm profiles, characteristic of nonporous material of low specific area. In general, the isotherms show profiles of type I (microporous) and type IV (hysteresis) adsorption, characteristic of microporous and mesoporous adsorbents, respectively. The calcination temperature considerably influences the textural properties of the materials.

The BET and micropore areas as well as the pore volume are shown in Table 2. As a general trend, the biochars produced from the chitosan HTC material showed higher surface areas compared with the CHIT-CO_3 adsorbents (Figure 4). The BET area increased from 466 to 2078 $m^2 \cdot g^{-1}$ upon increasing the pyrolysis temperature of the CHIT-CO_3 materials, whereas the area of the HTC48-CO_3 adsorbents varied from 1029 to

Table 2. Textural Properties of the Biochars Produced from Chitosan and HTC Chitosan

sample	BET area ($m^2 \cdot g^{-1}$)	micropore area ($m^2 \cdot g^{-1}$)[a]	micropore/ BET area (%)	pore volume ($cm^3 \cdot g^{-1}$)
chitosan	2.2			
CHIT-CO3-500	466	383	82	0.20
CHIT-CO3-600	913	809	89	0.37
CHIT-CO3-700	1647	1455	88	0.69
CHIT-CO3-800	2078	1603	77	0.88
CHIT-HTC48	2.6			
HTC48-CO3-500	1029	889	86	0.45
HTC48-CO3-600	1141	1002	88	0.48
HTC48-CO3-700	2262	1829	81	0.96
HTC48-CO3-800	2060	833	41	1.06

[a]Obtained by the t-plot method.

https://doi.org/10.1021/acs.energyfuels.5c02026
Energy Fuels XXXX, XXX, XXX−XXX

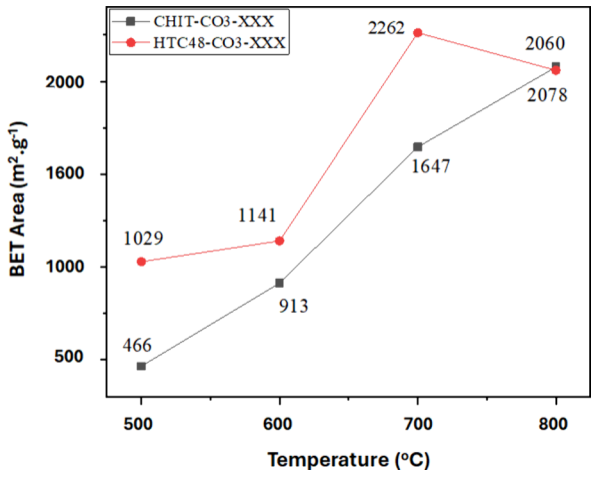

Figure 4. BET area of the biochars as a function of the calcination temperature.

2260 $m^2 \cdot g^{-1}$. An interesting behavior occurs at 800 °C; the area of the HTC48-CO3-800 adsorbent decreased relative to the material calcined at 700 °C, particularly the micropore area, which accounts for only 41% of the total BET area, about half of the contribution for the other HTC48-CO3 materials. Nevertheless, the pore volume and micropore area of these carbons increased with an enhancement of the activation temperature. These results indicate that at 800 °C some structural collapse occurs, which contributes to the decrease of microporosity. This may be due to the intense evolution of CO_2 and other gaseous species at this temperature. In fact, the SEM image of CHIT-CO3-700 shows a more porous structure, confirming the more intense gas evolution at 700 °C.

The results confirm that calcination of chitosan and the chitosan hydrochar in the range of 500 to 800 °C yields microporous carbons of high surface area. The release of gases during calcination generates microporosity, which passes through a maximum around 700 °C. Thus, increasing the calcination temperature leads to a partial collapse of the micropores and the formation of mesoporosity.

3.2. CO_2 Adsorption Experiments. The adsorption experiments were carried out at 25 °C and up to 1 bar of pure CO_2. The adsorption isotherms of the biochars and their precursors are shown in Figure S5 of the Supporting Information. Table 3 shows the total CO_2 uptake of the biochars at 1 bar and 25 °C. The values varied from 2.5 to 5.3 $mmol \cdot g^{-1}$ (110−233 $g \cdot kg^{-1}$). By contrast, the precursors showed significantly lower uptakes; chitosan presented only 0.1 $mmol \cdot g^{-1}$, whereas the chitosan hydrocar (CHIT-HTC48) showed 0.5 $mmol \cdot g^{-1}$.

Table 3. CO_2 Adsorption at 25 °C and 1 bar for the Chitosan Biochars

sample	CO_2 uptake ($mmol \cdot g^{-1}$)
chitosan	0.1
CHIT-CO3-500	2.5
CHIT-CO3-600	3.9
CHIT-CO3-700	5.3
CHIT-CO3-800	4.1
CHIT-HTC48	0.5
HTC48-CO3-500	3.5
HTC48-CO3-600	4.7
HTC48-CO3-700	4.5
HTC48-CO3-800	2.6

At least four chitosan biochars showed high efficiency for CO_2 capture, considering the value of 4.0 $mmol \cdot g^{-1}$ as a benchmark. The materials with the highest CO_2 uptake were CHIT-CO3-700 (5.3 $mmol \cdot g^{-1}$) and HTC48-CO3-600 (4.7 $mmol \cdot g^{-1}$) considering the overall uptake. The carbons derived from CHIT-HTC48 hydrochar, in the ranges of 500 and 600 °C, have higher adsorption values than those derived from the direct carbonization of chitosan. That occurred due to the increase in specific area and nitrogen content, combined with the effect of the microporosity in this range of activation temperature that can synergistically favor the interaction of the CO_2 molecule with the surface.

It is worth commenting on the lower adsorption capacity of the HTC48-CO3-800 biochar, compared with HTC48-CO3-600 and HTC48-CO3-700 biochars, in spite of its surface area above 2000 $m^2 \cdot g^{-1}$. As pointed out before, calcination at 800 °C seems to favor a partial collapse of the structure, affecting the microporosity. Indeed, HTC48-CO3-800 biochar presented only 833 $m^2 \cdot g^{-1}$ of micropore area, corresponding to 41% of the total surface area. This value is inferior to the micropore area of the other two biochars, which explains the lower CO_2 uptake. In addition, the HTC48-CO3-800 biochar showed only 1.5 wt % of nitrogen in its elemental composition, which may also affect the interaction of the surface with the CO_2 molecule. In fact, the nitrogen content on the biochar seems to play an important role in the CO_2 adsorption. For instance, the CO_2 uptake of HTC48-CO3-600 was slightly higher than the uptake of HTC48-CO3-700, despite the BET area being half of this later biochar. On the other hand, the nitrogen content was 2-fold higher, which may compensate the poorer textural properties of the HTC48-CO3-600 biochar. It may be suggested that a balance between textural properties and nitrogen content is relevant for the performance of the biochars. Whereas HTC48-CO3-600 showed a remarkable CO_2 uptake of 4.7 $mmol \cdot g^{-1}$, with 5.6 wt % of nitrogen in its composition, the CHIT-CO3-500 showed only 2.5 $mmol \cdot g^{-1}$ of CO_2 uptake, although having 7.1 wt % of nitrogen on its elemental composition. This apparent discrepancy may be explained by the difference in surface area, which is more than 2-fold higher on the HTC48-CO3-600 biochar, reflecting the balance between textural properties and elemental analysis.

We selected CHIT-CO3-700 and HTC48-CO3-600 biochars for further experiments, as these materials presented the highest CO_2 uptake within their family. Figure 5 shows the results of scanning electron microscopy (SEM). Unlike chitosan and HTC hydrochar, the activated carbons have morphologies with significant porosity formed upon calcination in the presence of K_2CO_3. The HTC-CO3-600 material seems to have a more uniform porosity when compared to the CHIT-CO3-700 adsorbent. By contrast, chitosan shows a smooth morphology that may be interpreted in terms of the packing of the polysaccharide chains, forming a rather crystalline structure. The CHIT-HTC48 material shows a SEM image similar to the chitosan, but some rugosity can be seen, indicating that partial unpacking of the polysaccharide chains has occurred upon the hydrothermal treatment. The SEM results of chitosan and CHIT-HTC48 precursors can explain the low CO_2 uptake of these materials, since the packing of the polysaccharide chains may impair the adsorption on the internal basic sites, which remain

https://doi.org/10.1021/acs.energyfuels.5c02026
Energy Fuels XXXX, XXX, XXX−XXX

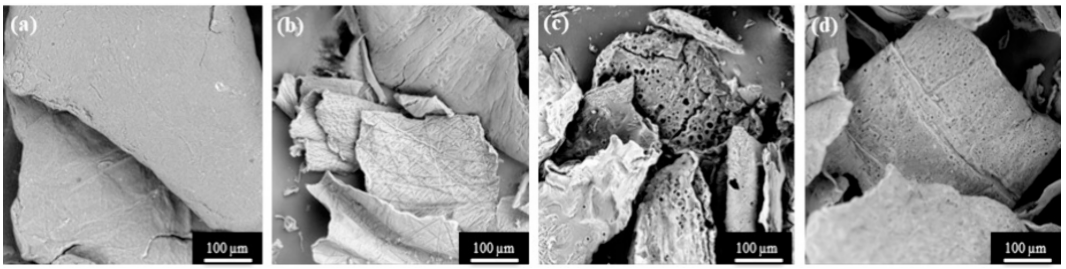

Figure 5. SEM images of (a) chitosan, (b) CHIT-HTC48, (c) CHIT-CO3-700, and (d) HTC48-CO_3-600.

inaccessible to the CO_2 molecules. Thus, only the more external basic sites may be available for CO_2 adsorption.

The basicity of the four adsorbents was assessed by means of a Boehm titration. The values are shown in Figure 6. The

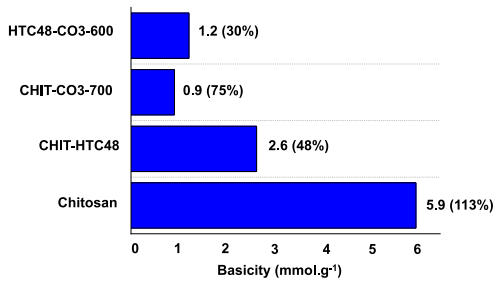

Figure 6. Basicity of the adsorbents from the Boehm titration. The number in parentheses represents the % of nitrogen atoms that contributes to the basicity.

parent chitosan presents the highest basicity, which roughly corresponds to 113% of the nitrogen atoms measured by CHN analysis. The result indicates that the packing of the polysaccharide chains is being destroyed in the acidic medium, liberating the NH_2 groups of the polysaccharide to neutralize them by the acid solution. The measured basicity was above the total N content, but this may be explained by some errors in the titration or in the CHN measurement, as well as upon protonation of part of the hydroxyl groups of the chitosan structure. On the other hand, the CHIT-HTC48 material shows about half of the nitrogen atoms available for neutralization by the acid solution. This may indicate that the HTC treatment may have partially transformed the NH_2 groups of the chitosan structure into N-pyridone and pyrrol-like structures of low basicity, which are not normally titrated by diluted acid solutions.

The basicity of the biochars was considerably lower when compared with the precursors. However, the basicity of the CHIT-CO_3-700 material correlates with about 75% of the nitrogen atoms of the adsorbent, according to the CHN measurements, whereas for the HTC48-CO3-600 the basicity accounts for only 30% of the nitrogen atoms. Again, the biochar produced from the calcination of HTC chitosan shows a poor correlation between the basicity and the nitrogen content, suggesting that the nitrogen atoms may be present as N-pyridone and pyrrole-like groups, a point that was supported by the FTIR measurements (Figure 3). Nevertheless, the HTC48-CO_3-600 biochar shows more basic sites per unit of mass than the CHIT-CO3-700, which may imply more sites for CO_2 chemisorption.

Table 4 shows the CO_2 uptake at different temperatures for CHIT-CO3-700 and HTC48-CO3−600 biochars. The data

Table 4. CO_2 Uptake of CHIT-CO3-700 and HTC48-CO3-600 Biochars at Different Temperatures

	CO_2 uptake (mmol·g^{-1})				
biochar	0 °C	15 °C	25 °C	40 °C	60 °C
CHIT-CO3-700	8.1	6.0	5.3	3.7	2.5
HTC48-CO3-600	7.4	5.9	4.7	3.9	2.9

were fitted by the Langmuir and Freundlich models. The parameters and correlation coefficients of the Langmuir model for each material are summarized in Tables 5 and 6, whereas

Table 5. Parameters of the Langmuir and Freundlich Models for the Adsorption of CO_2 on CHIT-CO3-700 at Different Temperatures

	Langmuir			
	temp (°C)	K_L (bar^{-1})	q_m (mmol·g^{-1})	r^2
CHIT-CO3-700	0	2.5	11	0.985
	25	1.5	8.5	0.976
	40	1.3	6.5	0.971
	60	1.1	4.6	0.951
	Freundlich			
	temp (°C)	K_F (mmol·g^{-1}·bar^{-1})	n	r^2
CHIT-CO3-700	0	8.2	2	0.998
	25	5.4	1.6	0.999
	40	3.8	1.5	0.999
	60	2.5	1.4	0.999

Figure S6 of the Supporting Information shows the linear representations of the Langmuir adsorption model for the two biochars. One can see a clear deviation from the linearity,

Table 6. Parameters of the Langmuir and Freundlich Models for the Adsorption of CO_2 on HTC48-CO3-600 at Different Temperatures

	Langmuir			
	temp (°C)	K_L (bar^{-1})	q_m (mmol·g^{-1})	r^2
HTC48-CO3-600	0	2.6	10	0.993
	25	2.2	6.6	0.983
	40	2.1	5.6	0.979
	60	1.8	4.3	0.964
	Freundlich			
	temp (°C)	K_F (mmol·g^{-1}·bar^{-1})	n	r^2
HTC48-CO3-600	0	7.7	2	0.995
	25	4.8	1.9	0.998
	40	3.9	1.8	0.999
	60	2.9	1.7	0.999

https://doi.org/10.1021/acs.energyfuels.5c02026
Energy Fuels XXXX, XXX, XXX−XXX

especially at 40 and 60 °C. The linear correlation coefficients (r^2) reduced from 0.985, at 0 °C, to 0.951, at 60 °C, for CHIT-CO_3-700, and from 0.993, at 0 °C, to 0.964, at 60 °C, for HTC-48-CO3-600, confirming that the Langmuir model did not adequately describe the adsorption process upon increasing the temperature. This is probably due to the heterogeneity of the biochar surfaces, which is not considered in this model. The values of the Langmuir constant (K_L) and the maximum adsorption capacity corroborate the exothermic nature of the CO_2 adsorption process on the biochars. From the K_L constants, it can be seen that the equilibrium on CHIT-CO3-700 was more affected by the temperature than on HTC48-CO3-600. These results suggest that chemisorption may play a more important role on HTC48-CO3−600 as the temperature increases.

Tables 5 and 6, as well as Figure S7, show the linear representations of the Freundlich adsorption model for the biochars obtained by linear regression. The results indicated that both materials show a better fit with this model, compatible with a more heterogeneous surface. These results agree with the chemical structure and textural properties of the biochars. The K_F parameters and the n factor reduced upon increasing the temperature, also corroborating the exothermic nature of the process. At all temperatures, the n factor was always greater than 1, indicating the heterogeneity of the sites, which could suggest a predomination of physisorption on the materials. The decrease of this parameter with the increase of the temperature suggests that chemisorption may play a more significant role at these conditions.[36] Nevertheless, this parameter cannot be solely used to distinguish between chemisorption and physisorption processes but might serve as an additional indicator.

From the adsorption isotherms at different temperatures, we could obtain enthalpy and entropy as well as the Gibbs free energy of the CO_2 adsorption on the biochars, using the Lagmuir model and the van't Hoff equation. The results are shown in Table 7 and the linearized plots are presented in Figure S8 of the Supporting Information. One can see that CHIT-CO_3-700 presents a more exothermic adsorption while showing a more prominent reduction in the entropy. Although these data should be interpreted with care, because the adsorption isotherms of both biochars are not well fitted by the Langmuir model, they may express the textural properties of the materials. The micropore area of CHIT-CO3-700 is higher than the micropore area of HTC48-CO3-600. The results suggest that microporosity plays a more important role in the CO_2 adsorption on CHIT-CO3-700, resulting in higher enthalpy of adsorption and more severe entropy reduction when compared to the HTC48-CO3-600 biochar.

Table 7. Thermodynamic Parameters of the CO_2 Adsorption on the Biochars

biochar	$\Delta G°$ (kJ mol^{-1})[a]	ΔH (kJ mol^{-1})	ΔS (J·K^{-1}·mol^{-1})
CHIT-CO3-700	−1.0	−10.4	−30.8
HTC48-CO3-600	−1.9	−4.5	−8.4

[a]Obtained at 298.15 K.

The isosteric heat was obtained using the Clausius−Clapeyron equation and is associated with the strength of the interaction between the adsorbate and the surface at different surface coverages. Figure 7 shows the isosteric heat (Q_{st}) against the amount of adsorbed CO_2 (q_{CO2}), whereas Figures S9 and S10 shows the linearized plots. The values varied between 20 and 29 kJ mol^{-1} for CHIT-CO3-700 and 13−28 kJ mol^{-1} for HTC-48-CO3-600 materials. The results stress the stronger adsorption of CO_2 on CHIT-CO3-700 biochar, as observed from the enthalpy of adsorption. The range of the values are similar to other chitosan biochars and the shape of the curves indicates the heterogeneity of the surface, as observed in other materials.[37−40]

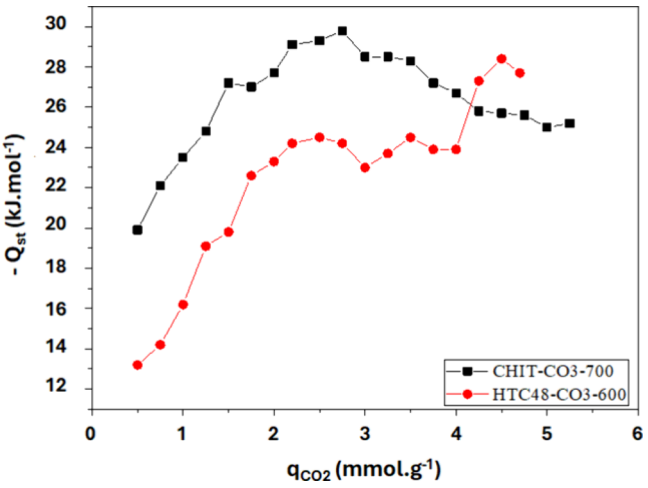

Figure 7. Isosteric heat (Q_{st}) against the amount of CO_2 adsorbed for CHIT-CO3-700 and HTC48-CO3-600 biochars.

The kinetics of CO_2 adsorption was also studied at different temperatures. Figure S11 shows the plots, whereas the fitting of the data, considering the pseudo-first- and pseudo-second-order models, are shown in Tables 8 and 9 for CHIT-CO3-700 and HTC48-CO3-600 biochars, respectively. Yet, the linearized plots of the pseudo-first- and pseudo-second-order models are shown in Figures S12 and S13 of the Supporting Information. The results show a slightly better fitting with the pseudo-second-order model. It has been proposed that the pseudo-first-order kinetic model is more associated with mass transfer and diffusion processes.[41] The kinetic constant (k_1) is basically the same for both biochars at the range of temperature studied, implying that mass transfer and diffusion of the CO_2 molecules present similar patterns on both materials. The kinetic constants were slightly higher than the values reported in the literature for CO_2 adsorption on pine

Table 8. Kinetic Parameters for the Adsorption of CO_2 on CHIT-CO3-700 at Different Temperatures and 1 bar

	pseudo first order			
	temp (°C)	k_1 (min^{-1})	q_e (mmol·g^{-1})	r^2
CHIT-CO3-700	0	0.76	9.7	0.991
	25	0.76	6.4	0.991
	40	0.76	4.1	0.991
	60	0.77	2.8	0.991
	pseudo second order			
	temp (°C)	k_2 (mmol·g^{-1}·min^{-1})	q_e (mmol·g^{-1})	r^2
CHIT-CO3-700	0	0.11	9.1	0.996
	25	0.17	5.9	0.996
	40	0.24	4.1	0.998
	60	0.35	2.8	0.998

https://doi.org/10.1021/acs.energyfuels.5c02026
Energy Fuels XXXX, XXX, XXX−XXX

Table 9. Kinetic Parameters for the CO_2 Adsorption on HTC-48-CO3-600 at Different Temperatures and 1 bar

	pseudo first order			
	temp (°C)	k_1 (min^{-1})	q_e ($mmol \cdot g^{-1}$)	r^2
HTC48-CO3-600	0	0.77	8.8	0.991
	25	0.77	5.6	0.991
	40	0.77	4.6	0.991
	60	0.77	3.5	0.991
	pseudo second order			
	temp (°C)	k_2 ($mmol \cdot g^{-1} \cdot min^{-1}$)	q_e ($mmol \cdot g^{-1}$)	r^2
HTC48-CO3-600	0	0.12	8.3	0.996
	25	0.19	5.2	0.996
	40	0.23	4.3	0.996
	60	0.31	3.2	0.996

sawdust hydrochars.[42] On the other hand, the pseudo-second-order kinetic model may be more associated with the interaction of the CO_2 molecule with the adsorption sites.[43,44] Overall, both biochars present similar kinetic constants (k_2), implying similar adsorption sites. The energy of activation, calculated from the kinetic data at different temperatures, was +17.2 $kJ \cdot mol^{-1}$ for CHIT-CO3-700 and +12.2 $kJ \cdot mol^{-1}$ for HTC48-CO3-600 biochar. The small difference also confirms the similar nature of the adsorption sites on both carbons.

The Fick and Linear Driving Force models were also applied to describe the kinetics of CO_2 adsorption on the biochars. However, the correlation coefficients (r^2) were poorer when compared with the pseudo-first- and pseudo-second-order models. For CHIT-CO3-700, the Fick diffusion coefficient (Dc) was 1.5×10^{-7} $cm^2 \cdot s^{-1}$ ($r^2 = 0.961$), whereas the mass transfer coefficient (k) of the linear driving force model was 0.030 s^{-1} ($r^2 = 0.908$), both at 25 °C and 1 bar. For HTC48-CO3-600 we found a Dc of 6.2×10^{-8} $cm^2 \cdot s^{-1}$ ($r^2 = 0.943$) and k of 0.021 s^{-1} ($r^2 = 0.969$). These values for the other two models were compatible with reported in the literature for other materials.[45−47]

3.3. Selective Adsorption of N_2 and CO_2. Figure 8 shows the N_2 and CO_2 adsorption isotherms at 25 °C and up to 1000 mbar for CHIT-CO3-700 and HTC-CO3-600 biochars, whereas Table 10 shows the Henry adsorption constants obtained upon linearization of the data up to 200 mbar (Figure S14). One can see that both materials are more selective to CO_2 than to N_2 adsorption. However, HTC-CO3-600 biochar presents a significantly higher selectivity than the CHIT-CO3-700 material. These results indicate that the HTC-CO3-600 biochar presents more chemisorption sites for CO_2 capture than the CHIT-CO3-700 biochar, as suggested by the Boehm titration (Figure 6). The higher N_2 uptake of CHIT-CO3-700 biochar may be explained by its higher surface area.

Figure 9 shows the results of the percentage of mass gain for the two biochars against the N_2/CO_2 gas composition in flow studies. The total mass gain and mass increment are shown in Tables S5 and S6 of the Supporting Information. The percentages of mass gain for pure N_2 are 0.04% and 0.19%, whereas the mass gains with 100% CO_2 are 15.68% and 16.09% for CHIT-CO_3-700 and HTC48-CO3-600 biochars, respectively. One can clearly see that at lower CO_2 concentrations the HTC48-CO3-600 biochar presents a higher percentage of mass gain than the CHIT-CO3-700 material. The results reinforce the presence of more chemisorption sites

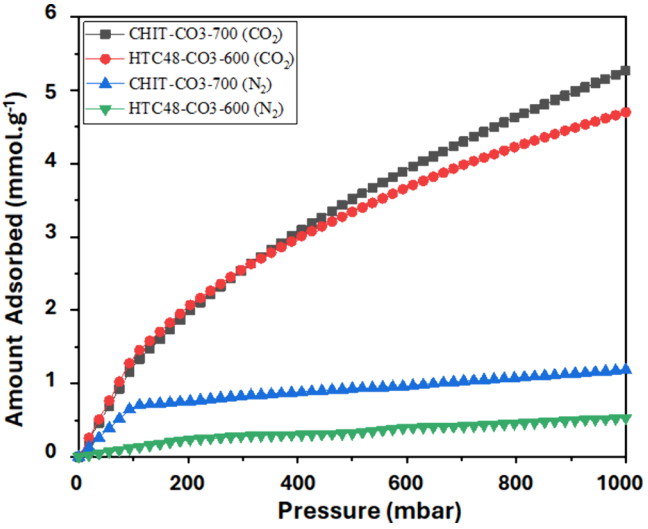

Figure 8. Adsorption isotherms for CO_2 and N_2 on activated carbons at 25 °C from 0 to 1 bar.

Table 10. Selectivity Factors of the Biochars Taken from the Adsorption Isotherms

sample	k_{CO2} [a]	k_{N2} [a]	selectivity [b]
CHIT-CO3-700	0.012	0.007	1.7
HTC48-CO3-600	0.013	0.0012	10

[a]Adsorption constant calculated from Henry's model (q = kP) within 0 to 200 mbar interval. [b]Selectivity factors calculated from the ratio of the adsorption constant ($S = k_{CO2}/k_{N2}$).

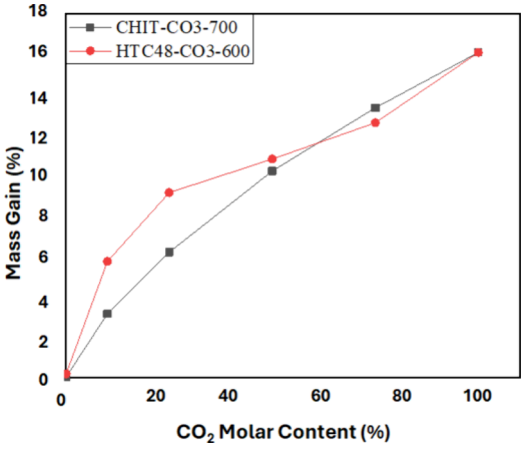

Figure 9. Mass gain (in percent) against the N_2/CO_2 molar composition of the flowing gas (0% means pure N_2).

on the HTC48-CO_3-600 biochar, as indicated by the Boehm titration and the selectivity factor. At higher CO_2 concentrations, the materials show similar adsorption properties, which may reflect the physisorption of the gas mixture on both materials, especially in the micropores.

3.4. Infrared Drifts of Adsorbed CO_2. Figures 10 and 11 show the *in situ* infrared spectra of adsorbed CO_2 on CHIT-CO3-700 and HTC48-CO3-600 biochars at different temperatures. One can clearly see the bands of the physisorbed CO_2 molecule, near 2340 and 660 cm^{-1}, associated with the asymmetric stretching and the bending vibrations, respectively, on the two biochars at 25 °C. Notwithstanding, as the temperature increases, these bands decrease in intensity but are

https://doi.org/10.1021/acs.energyfuels.5c02026
Energy Fuels XXXX, XXX, XXX−XXX

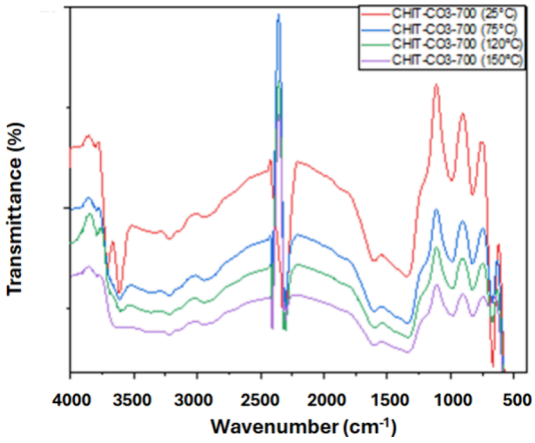

Figure 10. *In situ* infrared spectra of CHIT-CO3-700 under flowing CO_2 at different temperatures.

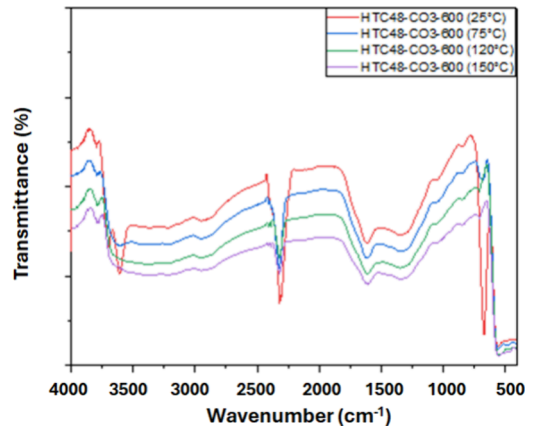

Figure 11. *In situ* infrared spectra of HTC48-CO3-600 under flowing CO_2 at different temperatures.

still present in the spectra of HTC48-CO3-600 even at 150 °C. However, they virtually disappear in the spectra of CHIT-CO3-700 at 75 °C and higher temperatures. Figures S15−S20 of the Supporting Information show an amplification of the infrared spectra at specific wavenumber regions. One can see a small shift to higher wavenumbers of the asymmetric CO_2 stretching on HTC48-CO3-600 as the temperature increases, indicating the weakness of the interaction of the CO_2 with the biochar surface. The same trend can also be observed for the bending of the CO_2 vibration near 660 cm^{-1}. On the other hand, for the CHIT-CO3-700 biochar, there is a clear difference in the spectra of CO_2 adsorbed at 25 °C and at higher temperatures. From the spectrum of the pure CHIT-CO3−700 biochar, it seems that some CO_2 may be trapped inside the pores, as small bands near 2300 and 660 cm^{-1} can be seen, similar to the pattern observed at 75 °C and higher temperatures. This fact may be related to the calcination procedure, where CO_2 may evolve from the system and become trapped inside the cavities that are formed.

An interesting point was observed in the infrared spectra of the biochars at 25 °C. There appears two more well-defined bands between 3600 and 3700 °C, whereas on the spectrum of the pure biochars there is a broad band in this region, which is characteristic of coal material, also indicating the presence of hydrogen bonds.[48,49] The exact nature of these two bands upon adsorption at 25 °C is not completely clear, but it may be associated with isolated phenol groups[50] that do not significantly interact with the CO_2 molecule.

3.5. Comparison with Literature Results of Other Chitosan-Carbon Adsorbents. Chitosan-based adsorbents have been already used on CO_2 capture.[30] Table 11 shows the CO_2 uptake of different chitosan-based materials. In all of these studies, the presence of microporosity was clearly indicated as important to achieve high CO_2 uptake. Compared with other chitosan biochars, the results of CO_2 capture with the materials prepared in this study are among the highest reported. In addition, in most of the previous studies, no kinetic analysis, basicity correlation, and selectivity measurements, as well as *in situ* spectroscopic studies, were reported.

There is basically one study that combines the hydrothermal chitosan carbonization and the subsequent activation at high temperature.[26] Initially, chitosan was autoclaved at 200 °C in an aqueous solution of acetic acid. The resulting hydrochar was then treated with different proportions of NaOH or KOH and directly calcined at 800 °C, resulting in the final biochar. The area of the hydrochar was 60 $m^2 \cdot g^{-1}$, whereas the final biochars presented areas varying from 263 to 4168 $m^2 \cdot g^{-1}$. The nitrogen content was 6.0 wt % in the hydrochar precursor and varied from 2.2 to 6.7 wt % in the calcined samples. The highest CO_2 uptake, of 5.4 $mmol \cdot g^{-1}$ at 25 °C and 1 bar, was observed with the CHKH1:3 biochar, prepared by the final calcination of the hydrochar with KOH at a 1:3 relative mass proportion. The nitrogen content of CHKH1:3 was 2.9 wt %, lower than the nitrogen content of HTC48-CO3-600 (5.6 wt %). Nevertheless, the BET area of CHKH1:3 was significantly higher, being 3226 $m^2 \cdot g^{-1}$, whereas HTC48-CO3-600 presents a BET area of 1141 $m^2 \cdot g^{-1}$. The CHK1:3 material presented a CO_2/N_2 selectivity of 55, higher than HTC48-CO3-600, in which the selectivity was 10. However, no result of CO_2 adsorption at lower pressures or concentrations were reported, and the authors associated the adsorption properties with the microporosity of the materials, implying that physisorption is mostly predominant. The CHIT-CO3-700 and HTC48-CO3-600

Table 11. Comparison of Different Chitosan-Carbon Materials for CO_2 Capture at 25 °C and 1 bar

adsorbent	preparation method	CO_2 uptake ($mmol \cdot g^{-1}$)	ref
NAC-Rb(600)	carbonization of chitosan-lactic acid with Rb_2CO_3 at 600 °C	4.9	29
AC-2-635	chitosan chemical activation with K_2CO_3 (2:1) at 635 °C	3.9	25
CUK-112	calcination of chitosan at 600 °C followed by chemical activation with KOH and urea at 800 °C	3.9	24
CHKH1:3	hydrothermal carbonization of chitosan followed by chemical activation with KOH (1:3) at 800 °C	5.4	26
CHI-G-900	carbonization of chitosan-acetic acid gel at 900 °C	3.6	27
CHIT-CO3-700	chitosan chemical activation with K_2CO_3 (1:1) at 700 °C	5.3	this work
HTC48-CO3-600	hydrothermal carbonization of chitosan at 180 °C followed by chemical activation with K_2CO_3 (1:1) at 600 °C	4.7	this work

https://doi.org/10.1021/acs.energyfuels.5c02026
Energy Fuels XXXX, XXX, XXX−XXX

materials prepared in this work presented significantly lower surface areas, but the CO_2 uptakes are similar or slightly lower. In addition, K_2CO_3 was used as an activating agent instead of KOH, and in significantly lower loadings. Another difference concerns the hydrothermal carbonization of the parent chitosan, which was carried out with pure water in the present study without the need for acetic acid in the medium. Finally, in the present study, an intermediate calcination at 300 °C was carried out before increasing to the desired final calcination temperature. This step seems to be important to preserving more nitrogen atoms on the HTC48-CO3-600 biochar.

Compared with the previous reports in the literature on the preparation and use of chitosan biochars for CO_2 capture, our results rank among the highest reported, with one of the most simple and sustainable procedures for their preparation. In addition, to the best of our knowledge, this is the first study to report kinetic analysis of CO_2 capture on chitosan biochars, which is important when considering these materials as potential commercial adsorbents for CO_2 gaseous streams and, especially, for use in DAC processes.

3.6. Perspective for the Biochars within DAC Applications. Direct air capture (DAC) has received increased attention in the past years. It is a good alternative to achieve negative CO_2 emissions in the future, to cope with the international climate agreements. Within this context, the use of chitosan biochars can be of great relevance but not for a straightforward use, as they mostly capture CO_2 by physisorption, while DAC requires more selective materials to adsorb gaseous concentrations as low as 420 ppm. However, the biochars can serve as excellent supports for further functionalization. The chitosan biochars are thermally stables at least up to 300 °C, ensuring good resistance to multiple adsorption and desorption cycles, which is of prime importance for commercial applications.

Chitosan is a byproduct of the seafood industry and is available in most parts of the world. The current price of chitosan produced from crustacean can vary from 10 to 1000 USD per kg and global sales were around 2.5 billion USD in 2024.[51] Today, chitosan is mostly used in the food[52] and biomedical[53] sectors. The potential use of chitosan in CCS and CCU processes may increase world production, also reducing the associated costs.

4. CONCLUSIONS

Chitosan biochars were prepared by two different methods. In the first, the parent chitosan was directly calcined in the presence of the same mass of K_2CO_3 through a two-step temperature program. First, the material was heated up to 300 °C, staying at this temperature for 30 min, and then to the final desired temperature (500 to 800 °C) to afford the final CHIT-CO3 biochars. The other method started from the chitosan hydrochar (CHIT-HTC48), which was treated by the same two-steps temperature program to yield HTC48-CO3 biochars. The materials obtained through the direct calcination of chitosan usually present lower nitrogen content and surface area and higher C/N atomic ratios.

The CO_2 uptake of the biochars ranged from 2.5 to 5.3 $mmol \cdot g^{-1}$, at 25 °C and 1 bar. Although the CHIT-CO3-700 biochar presented the highest CO_2 uptake among the tested materials, it is less selective to CO_2 than the HTC48-CO3-600 biochar, which showed an uptake of 4.7 $mmol \cdot g^{-1}$. These results may be explained by the higher nitrogen content and basicity of this later biochar, being more selective toward CO_2 capture by chemisorption, whereas CHIT-CO3-700 presents higher surface area. Thus, a correct balance between textural and compositional properties seems to be of prime importance to achieving high CO_2 uptakes.

The isotherms were better fitted by the Freundlich model, indicating a heterogeneous surface. The isosteric heat at different surface coverages confirmed the heterogeneous nature of the biochar surfaces. Both biochars presented similar pseudo-first-order constants, indicative of similar mass transfer kinetics. The results were better fitted by the pseudo-second-order kinetics, with CHIT-CO3-700 showing slightly higher energy of activation. The Fick and Linear Driving Force models were also applied to understanding the kinetics of CO_2 adsorption, but the fitting of the data was poorer compared with the pseudo-first- and pseudo-second-order models.

Flow experiments using different concentrations of CO_2 and N_2 showed the potential of both materials, but especially HTC48-CO3-600 biochar, for capturing CO_2 in diluted gas mixtures. The nitrogen content and basicity of the materials are of high importance in determining the CO_2 adsorption properties of the chitosan biochars.

In situ infrared studies of adsorbed CO_2 at different temperatures indicated that the HTC48-CO3-600 biochar may retain CO_2 on the surface up to at least 150 °C, whereas CHIT-CO3-700 seems to present some trapped CO_2 inside the pores during the preparation process.

The results indicated that high-efficient chitosan biochars can be preferentially prepared upon the chemical activation and calcination of the HTC chitosan, with an intermediate calcination at 300 °C, preserving more nitrogen atoms on the structure, while generating superior basicity necessary for the CO_2 chemisorption.

■ ASSOCIATED CONTENT

Supporting Information

The Supporting Information is available free of charge at https://pubs.acs.org/doi/10.1021/acs.energyfuels.5c02026.

Figures and tables with additional characterization and CO_2 uptake data of the adsorbents (PDF)

■ AUTHOR INFORMATION

Corresponding Author

Claudio J. A. Mota − *Universidade Federal do Rio de Janeiro, Instituto de Química, Rio de Janeiro 21941-909, Brazil; Universidade Federal do Rio de Janeiro, Escola de Química, Rio de Janeiro 21941-909, Brazil; INCT Energia e Ambiente, UFRJ, 21941-909 Rio de Janeiro, Brazil;* orcid.org/0000-0002-8130-1192; Email: cmota@iq.ufrj.br

Authors

José A. O. Chagas − *Universidade Federal do Rio de Janeiro, Instituto de Química, Rio de Janeiro 21941-909, Brazil; CarbonAir Energy, Rua Hélio de Almeida, Rio de Janeiro 21641-614, Brazil;* orcid.org/0000-0001-5252-2992

Bianca P. Pinto − *Universidade Federal do Rio de Janeiro, Instituto de Química, Rio de Janeiro 21941-909, Brazil; CarbonAir Energy, Rua Hélio de Almeida, Rio de Janeiro 21641-614, Brazil;* orcid.org/0000-0002-0645-5896

Ana Lúcia de Lima − *Universidade Federal do Rio de Janeiro, Instituto de Química, Rio de Janeiro 21941-909, Brazil*

Complete contact information is available at:

https://doi.org/10.1021/acs.energyfuels.5c02026
Energy Fuels XXXX, XXX, XXX−XXX

https://pubs.acs.org/10.1021/acs.energyfuels.5c02026

Funding

The Article Processing Charge for the publication of this research was funded by the Coordenacao de Aperfeicoamento de Pessoal de Nivel Superior (CAPES), Brazil (ROR identifier: 00x0ma614).

Notes

The authors declare no competing financial interest.

■ ACKNOWLEDGMENTS

Authors acknowledge financial support from FINEP, CNPq, CAPES, and FAPERJ. The NQTR (IQ-UFRJ) is acknowledged for SEM analyses.

■ REFERENCES

(1) Ghiat, I.; Al-Ansari, T. A review of carbon capture and utilisation as a CO_2 abatement opportunity within the EWF nexus. *J. CO_2 Util.* **2021**, *45*, 101432.
(2) McQueen, N.; Gomes, K. V.; McCormick, C.; Blumanthal, K.; Pisciotta, M.; Wilcox, J. A review of direct air capture (DAC): Scaling up commercial technologies and innovating for the future. *Prog. Energy* **2021**, *3*, 032001.
(3) Khan, U.; Ogbaga, C. C.; Abiodun, O.-A. O.; Adeleke, A. A.; Ikubanni, P. P.; Okoye, P. U.; Okolie, J. A. Assessing absorption-based CO_2 capture: Research progress and techno-economic assessment overview. *Carbon Capture Sci. Technol.* **2023**, *8*, 100125.
(4) Wang, N.; Wang, D.; Krook-Riekkola, A.; Ji, X. MEA-based CO_2 capture: a study focuses on MEA concentrations and process parameters. *Front. Energy Res.* **2023**, *11*, 1230743.
(5) Devaraja, D.; Kiss, A. A. Novel intensified process for ethanolamines production using reactive distillation and dividing-wall column technologies. *Chem. Eng. Proc. Proc. Inten.* **2022**, *179*, 109073.
(6) Anastas, P.; Eghbali, N. Green Chemistry: Principles and Practice. *Chem. Soc. Rev.* **2010**, *39*, 301−312.
(7) Raganati, F.; Miccio, F.; Ammendola, P. Adsorption of Carbon Dioxide for Post-combustion Capture: A Review. *Energy Fuel* **2021**, *35*, 12845−12868.
(8) Mahajan, S.; Lahtinen, M. Recent progress in metal-organic frameworks (MOFs) for CO_2 capture at different pressures. *J. Environ. Chem. Eng.* **2022**, *10*, 108930.
(9) Zulkifli, Z. I.; Lim, K. L.; Teh, L. P. Metal-Organic Frameworks (MOFs) and their Applications in CO_2 Adsorption and Conversion. *ChemistrySelect* **2022**, *7*, 202200572.
(10) Liu, L.; Jin, S.; Ko, K.; Kim, H.; Ahn, I. S.; Lee, C. H. Alkyl-Functionalization of (3-Aminopropyl)Triethoxysilane-Grafted Zeolite Beta for Carbon Dioxide Capture in Temperature Swing Adsorption. *Chem. Eng. J.* **2020**, *382*, 122834.
(11) Boer, D. G.; Langerak, J.; Pescarmona, P. P. Zeolites as Selective Adsorbents for CO_2 Separation. *ACS Appl. Energy Mater.* **2023**, *6*, 2634−2656.
(12) Licciulli, A.; Notaro, M.; De Santis, S.; Terreni, C.; Padmanabhan, S. K. CO_2 Capture on Amine Impregnated Mesoporous Alumina-Silica Mixed Oxide Spheres. *Fuel Process. Technol.* **2017**, *166*, 202−208.
(13) Irani, M.; Jacobson, A. T.; Gasem, K. A. M.; Fan, M. Synthesized Porous Polymer as Support of Poly(Ethyleneimine) for Effective CO_2 Capture. *Energy* **2018**, *157*, 1−9.
(14) Hu, X.; Liu, L.; Luo, X.; Xiao, G.; Shiko, E.; Zhang, R.; Fan, X.; Zhou, Y.; Liu, Y.; Zeng, Z.; Li, C. A Review of N-Functionalized Solid Adsorbents for Post-Combustion CO_2 Capture. *Appl. Energy* **2020**, *260*, 114244.
(15) Sanz-Pérez, E. S.; Murdock, C. R.; Didas, S. A.; Jones, C. W. Direct Capture of CO_2 from Ambient Air. *Chem. Rev.* **2016**, *116*, 11840−11876.
(16) Chagas, J. A. O.; Marciniak, A. A.; Mota, C. J. A. Trends in Carbon Dioxide Capture and Conversion. *J. Braz. Chem. Soc.* **2022**, *23*, 801−814.
(17) Sircar, S.; Golden, T. C.; Rao, M. B. Activated Carbon for Gas Separation and Storage. *Carbon* **1996**, *34*, 1−12.
(18) Coromina, H. M.; Walsh, D. A.; Mokaya, R. Biomass-derived activated carbon with simultaneously enhanced CO_2 uptake for both pre and post combustion capture application, J. *Mater. Chem. A* **2016**, *4*, 280−289.
(19) Jedli, H.; Almonnef, M.; Rabhi, R.; Mbarek, M.; Abdessalem, J.; Slimi, K. Activated Carbon as an Adsorbent for CO_2 Capture: Adsorption, Kinetics, and RSM Modeling. *ACS Omega* **2024**, *9*, 2080−2087.
(20) Guo, Y.; Tan, C.; Sun, J.; Li, W.; Zhang, J.; Zhao, C. Porous activated carbons derived from waste sugarcane bagasse for CO_2 adsorption. *Chem. Eng. J.* **2020**, *381*, 122736.
(21) Rashidi, N. A.; Yusup, S. Potential of palm kernel shell as activated carbon precursors through single stage activation technique for carbon dioxide adsorption. *J. Cleaner Prod.* **2017**, *168*, 474−486.
(22) Ali, G. A. M.; Habeeb, O. A.; Algarni, H.; Chong, K. F. CaO impregnated highly porous honeycomb activated carbon from agriculture waste: symmetrical supercapacitor study. *J. Mater. Sci.* **2019**, *54*, 683−692.
(23) Chin, B. L. F.; Loy, A. C. M. K.; Cheah, W.; Chan, Y. H.; Lock, S. S. M.; Yiin, C. L. Graphene-based nanomaterials for CO_2 capture and conversion. *Nanomaterials for Carbon Dioxide Capture and Conversion Technologies*; ScienceDirect, 2023, Chapter 8, pp 211−243.
.
(24) Rehman, A.; Park, S. From chitosan to urea-modified carbons: Tailoring the ultra-microporosity for enhanced CO_2 adsorption. *Carbon* **2020**, *159*, 625−637.
(25) Fan, X.; Zhang, L.; Zhang, G.; Shu, Z.; Shi, J. Chitosan derived nitrogen-doped microporous carbons for high performance CO_2 capture. *Carbon* **2013**, *61*, 423−430.
(26) Kamran, U.; Park, S. Tuning ratios of KOH and NaOH on acetic acid-mediated chitosan-based porous carbons for improving their textural features and CO_2 uptakes. *J. CO_2 Util.* **2020**, *40*, 101212.
(27) Barroso-Martin, I.; Cecilia, J. A.; Vilarrasa-Garcia, E.; Ballesteros-Plata, D.; Jimenez-Gomez, C. P.; Vilchez-Cozar, A.; Infantes-Molina, A.; Rodriguez-Castellon, E. Modification of the Textural Properties of Chitosan to Obtain Biochars for CO_2-Capture Processes. *Polymers* **2022**, *14*, 5240.
(28) Li, D.; Zhou, J.; Zhang, Z.; Li, L.; Tian, Y.; Lu, Y.; Qiao, Y.; Li, J.; Wen, L. Improving low-pressure CO_2 capture performance of N-doped active carbons by adjusting flow rate of protective gas during álcali activation. *Carbon* **2017**, *114*, 496−503.
(29) Fujiki, J.; Yogo, K. The increased CO_2 adsorption performance of chitosan-derived activated carbons with nitrogen-doping. *Chem. Commun.* **2016**, *52*, 186−189.
(30) Foong, S. Y.; Chan, Y. H.; Yiin, C. L.; Lock, S. S. M.; Loy, A. C. M.; Lim, J. Y.; Yek, P. N. Y.; Mahari, W. A. W.; Liew, R. K.; Peng, W.; Tabatabaei, M.; Aghbashlo, M.; Lam, S. S. Sustainable CO_2 capture via adsorption by chitosan-based functional biomaterial: A review on recent advances, challenges, and future directions. *Renew. Sustain. Energy Rev.* **2023**, *181*, 113342.
(31) Zhang, C.; Song, W.; Ma, Q.; Xie, L.; Zhang, X.; Guo, H. Enhancement of CO_2 Capture on Biomass-Based Carbon from Black Locust by KOH Activation and Ammonia Modification. *Energy Fuels* **2016**, *30*, 4181−4190.
(32) Chen, T.; Deng, S.; Wang, B.; Huang, J.; Wang, Y.; Yu, G. CO_2 Adsorption on Crab Shell Derived Activated Carbons: Contribution of Micropores and Nitrogen-Containing Groups. *RSC Adv.* **2015**, *5*, 48323−48330.
(33) Chagas, J. A. O.; Crispim, G. O.; Pinto, B. P.; San Gil, R. A. S.; Mota, C. J.A. Synthesis, Characterization and CO_2 Uptake of Adsorbents Prepared by Hydrothermal Carbonization of Chitosan. *ACS Omega* **2020**, *5*, 29520−29529.
(34) Oliveira, D. E. F.; Chagas, J. A. O.; de Lima, A. L.; Mota, C. J. A. CO_2 Capture over MCM-41 and SBA-15 Mesoporous Silicas

Impregnated with Chitosan. *Ind. Eng. Chem. Res.* **2022**, *61*, 10522−10530.
(35) Olejniczak, A.; Lezanska, M.; Wloch, J.; Kucinska, A.; Lukaszewicz, J. P. Novel nitrogen-containing mesoporous carbons prepared from chitosan. *J. Mater. Chem.* **2013**, *1*, 8961−8967.
(36) Chowdhury, S.; Mishra, R.; Saha, P.; Kushwaha, P. Adsorption thermodynamics, kinetics and isosteric heat of adsorption of malachite green onto chemically modified rice husk. *Desalination* **2011**, *265*, 159−168.
(37) Kayal, S.; Teo, H. W. B.; Chakraborty, A. Prediction of phase transitions by investigating CO_2 adsorption on 1% lithium doped MIL-101 (Cr) MOF with anomalous type isosteric heat of adsorption. *Micro. Meso. Mater.* **2016**, *236*, 21−27.
(38) Tiwari, D.; Goel, C.; Bhunia, H.; Bajpai, P. K. Dynamic CO_2 capture by carbon adsorbents: Kinetics, isotherm and thermodynamic studies. *Sep. Pur. Technol.* **2017**, *181*, 107−122.
(39) Singh, J.; Bhunia, H.; Basu, S. CO_2 adsorption on oxygen enriched porous carbon monoliths: Kinetics, isotherm and thermodynamic studies. *J. Ind. Eng. Chem.* **2018**, *60*, 321−332.
(40) Zheng, Y.; Li, Q.; Yuan, C.; Tao, Q.; Zhao, Y.; Zhang, G.; Liu, J. Influence of temperature on adsorption selectivity: Coal-based activated carbon for CH_4 enrichment from coal mine methane. *Powder Technol.* **2019**, *347*, 42−49.
(41) Loganathan, S.; Tikmani, M.; Edubilli, S.; Mishra, A.; Ghoshal, A. K. CO_2 adsorption kinetics on mesoporous silica under wide range of pressure and temperature. *Chem. Eng. J.* **2014**, *256*, 1−8.
(42) Vega, M. F.; Díaz-Faes, E.; Barriocanal, C. Kinetic and Mechanistic Study of CO_2 Adsorption on Activated Hydrochars. *J. CO_2 Util.* **2024**, *81*, 102716.
(43) Ho, Y. S.; Mckay, G. Sorption of dye from aqueous solution by peat. *Chem. Eng. J.* **1998**, *70*, 115−124.
(44) Song, G.; Zhu, X.; Chen, R.; Liao, Q.; Ding, Y. D.; Chen, L. An investigation of CO_2 adsorption kinetics on porous magnesium oxide. *Chem. Eng. J.* **2016**, *283*, 175−183.
(45) Garcés-Polo, S. I.; Villarroel-Rocha, J.; Sapag, K.; Korili, S. A.; Gil, A. A Comparative Study of CO_2 Diffusion from Adsorption Kinetic Measurements on Microporous Materials at Low Pressures and Temperatures. *Chem. Eng. J.* **2016**, *302*, 278−286.
(46) Rupa, M. J.; Pal, A.; Mitra, S.; Saha, B. B. Time Adapted Linear Driving Force Model for Gas Adsorption onto Solids. *Chem. Eng. J.* **2021**, *420*, 129785.
(47) Wang, Y.; Zhao, D.; Li, G. K. Temperature-dependent Kinetic Analysis of Direct Air Capture Using a Gravimetric Approach in Porous Environments. *Adsorption* **2025**, *31*, 71.
(48) Acevedo, S.; Giraldo, L.; Moreno-Piraján, J. C. Adsorption of CO_2 on Activated Carbons Prepared by Chemical Activation with Cupric Nitrate. *ACS Omega* **2020**, *5*, 10423−10432.
(49) Janu, R.; Mrlik, V.; Ribitsch, D.; Hofman, J.; Sedlácek, P.; Bielská, L.; Soja, G. Biochar surface functional groups as affected by biomass feedstock, biochar composition and pyrolysis temperature. *Carbon Resour. Conv.* **2021**, *4*, 36−46.
(50) Cannon, S. A.; Chu, C. J.; Hauge, R. H.; Margrave, J. L. Infrared absorption characteristics of hydroxyl groups in coal tars. *Fuel* **1987**, *66*, 51−54.
(51) Huq, T.; Khan, A.; Brown, D.; Dhayagude, N.; He, Z.; Ni, Y. Sources, Production and Commercial Applications of Fungal Chitosan: A Review. *J. Bioresour. Bioprod.* **2022**, *7*, 85−98.
(52) Shahbaz, U.; Basharat, S.; Javed, U.; Bibi, A.; Yu, X. B. Chitosan: a Multipurpose Polymer in Food Industry. *Polymer Bull.* **2023**, *80*, 3547−3569.
(53) Harugade, A.; Sherje, A. P.; Pethe, A. Chitosan: A Review on Properties, Biological Activities and Recent Progress in Biomedical Applications. *Reactive Funct. Polymers* **2023**, *191*, 105634.

https://doi.org/10.1021/acs.energyfuels.5c02026
Energy Fuels XXXX, XXX, XXX−XXX